This article has been accepted for publication in a future issue of this journal, but has not been fully edited. Content may change prior to final publication. Citation information: DOI 10.1109/TMECH.2016.2529664, IEEE/ASME Transactions on Mechatronics



# AnyClimb: A New Wall-Climbing Robotic Platform for Various Curvatures

Yanheng Liu, HyunGyu Kim, and TaeWon Seo, *Member, IEEE*

***Abstract*— Climbing robots are being developed to clean, paint, or inspect high areas that are hard to reach for human beings. To widen their application area, robotic platforms have been suggested using bio-inspired attachment methods, such as dry and wet adhesion for smooth and rough surfaces. Generally, robots can climb either walls or poles, but there has been no single robotic platform that can climb both. We developed a new robotic platform to vertically climb a surface with various curvatures in the horizontal direction. Flat dry adhesive was used to make eight footpads. Walking locomotion of the footpads was achieved by a four-bar mechanism with a single motor. To adapt to curved walls, a compliant mechanism is suggested with an asymmetric four-bar mechanism. The kinematics and compliance design parameters were determined by analysis, and experiments were performed on walls with different curvatures. We plan to apply the platform to clean the surfaces of solar panels with different curvatures after modifying the design for commercialization.**

***Index Terms*—Wall-climbing robot, Dry adhesion, Compliant mechanism, Four-bar mechanism, Curvature.**

## I. Introduction

Wall-climbing robots (WCRs) have been developed for various practical applications, such as cleaning high-rise buildings [1] and painting the outer walls of ships [2]. Generally, vacuum suction, wire supports, and magnetic attachments are used to maintain the vertical position [3]. The attachment methods have limitations of high energy consumption, noise (from vacuums), low agility (from wire support), and limited attachment ability on ferromagnetic surfaces. These characteristics limit the application of WCRs.

To expand the application area of WCRs, several attachment methods that are generally bio-inspired have been suggested recently. Gecko-inspired dry adhesion is a very popular research area [4-6]. The adhesion method uses the van der Waals force of micro/nano fibers to attach to very smooth surfaces. Claws are also a very interesting attachment method for rough surfaces [7, 8]. The claw mechanism is used to climb walls by imitating insects and animals [9, 10]. Flat dry adhesives such as V-10 were suggested by some researchers [11, 12]. This method has advantages of adhesion to various materials and structure surfaces, but contamination is a remaining challenge. Wet adhesion with glues was proposed recently with inspiration from ants [13], which solved the contamination problem of dry adhesives. However, wet adhesion leaves glue on the surface, and the applicable areas are very limited.

Many robotic platforms for wall climbing with bio-inspired adhesion have been developed recently [14]. Seo and Sitti [11] proposed a tank-like module-based WCR with flat dry adhesives. The robot used compliant motion to overcome large obstacles. Spenko et al. [15] developed a hexapedal climbing robotic platform called RiSE, which can climb a rough vertical surface using a bio-inspired attachment unit with spines. Parness and McKenzie [8] proposed a wheel-based robot with multiple micro-spines to climb a flat vertical surface. The robot can also climb stairs with wheel locomotion. Murphy and Sitti [16] presented a compact WCR called Waalbot for the inspection of airplanes using gecko-inspired micro fibers to adhere to the smooth surfaces. Contamination and overcoming obstacles are remaining challenges for the commercialization of bio-inspired WCRs.

External pipe climbing is one important issue for climbing robots. Generally, pipe climbing is used for inspecting pipes or ropes. Lee [17] suggested such a climbing robot for pipe inspection. The robot can climb pipes with various diameters by independently controlling adjustable driving wheels. Cho et al. [18] developed a rope-climbing robot for bridge inspection using a triangular wheel mechanism to maintain the weight against the force of gravity, which was similar to Lee's method [17]. Haynes et al. [19] tried a different approach using an inward claw to climb a wooden pole. The method reliably supports the weight of the robot, but scratches remain on the pole. Guan et al. [20] proposed a pole-climbing robot with four serial linkages and grippers at the ends. The robot was limited by the size of the poles due to the limited size of the grippers.

This paper proposes a new vertical climbing robotic platform called AnyClimb for walls and poles with a single configuration. As far as we know, there is no dry adhesive-based climbing robot that can achieve this with a single platform. The robot uses flat dry adhesives to attach to surfaces. To adapt to walls with various curvatures, a compliant mechanism is used based on an asymmetric four-bar mechanism. The vertical walking locomotion of the robot is achieved by the four-bar mechanism, while the compliant mechanism adapts to the surface geometry. The parametric design and experimentally optimized dry adhesive footpads are presented.

The rest of this paper is organized as follows. Section II describes the mechanical configuration of AnyClimb, and the

This study was supported by a National Research Foundation of Korea (NRF) grant funded by the Ministry of Future, ICT and Planning of the Korean government (no. 2015M2A8A4049951).

Y. Liu, H. Kim and T. Seo are with Creative Robot Design Lab., School of Mechanical Engineering, Yeungnam University, Gyeongsan 712-749, Korea (e-mail: liuyanheng0730@nate.com, hyungyu 8066@naver.com, and taewon _seo@yu.ac.kr(corresponding author)).

*Y. Liu and H. Kim made equal contributions as a first author.

This article has been accepted for publication in a future issue of this journal, but has not been fully edited. Content may change prior to final publication. Citation information: DOI 10.1109/TMECH.2016.2529664, IEEE/ASME Transactions on Mechatronics



locomotion and adaptation strategies are explained. Section III presents the optimization procedure and results of the dry adhesive footpads. The parameters were examined by experiments for robust adhesion ability on various surfaces. Section IV presents the parametric design of AnyClimb. Kinematic parameters and compliance parameters were determined by analysis. Failure analysis of the robot platform is presented in Section V based on force and moment equilibrium equations. The prototype assembly and experimental results on the climbing ability are presented in Section VI. Conclusions follow in Section VII.

## II. AnyClimb Mechanism and Locomotion

The configuration of AnyClimb is shown in Fig. 1. The robot is composed of two rectangular frames, each with four dry adhesive footpads. The frames are connected by a parallel four-bar linkage mechanism. Based on the mechanism, the robot can climb a vertical wall by sequential walking locomotion, as shown in Fig. 2. The inner and outer rectangular frames are moved in the vertical direction sequentially based on the four-bar mechanism. The locomotion is achieved by a single motor, and the two actuated axes are operated simultaneously using a bevel gear and timing belt. In addition, the robot can climb down by operating the motor in opposite direction. A tail is implemented at the end of the robot to reduce the pitch-back moment. Note the tail should point downward while the robot climbs up or down due to the pitch-back moment.

The mechanism for adapting to various curvatures is very important for vertical climbing on walls and poles. The mechanism is shown in Fig. 3 and is composed of two symmetric trapezoidal four-bar mechanisms. The two mechanisms are used to adapt to various curvatures. Since the preloads are determined by the compliant force, the design of the compliance parameters is very important. During the detachment process, the mechanically limited four-bar linkage makes a sufficient force for the detachment of the dry adhesives.

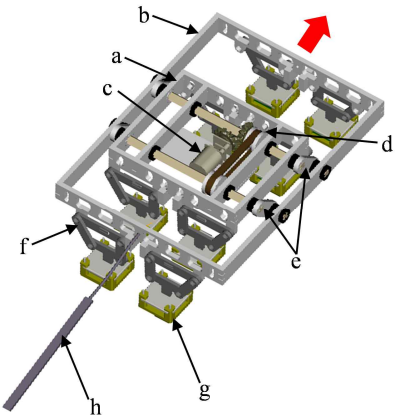


Fig. 1. Mechanical configuration of AnyClimb: a) inner frame, b) outer frame c) motor and bevel gear, d) timing belt and pulley, e) parallel four-bar mechanism, f) trapezoidal four-bar mechanism, g) foot-pads, h) tail. Red arrow denotes the moving direction of the robot.

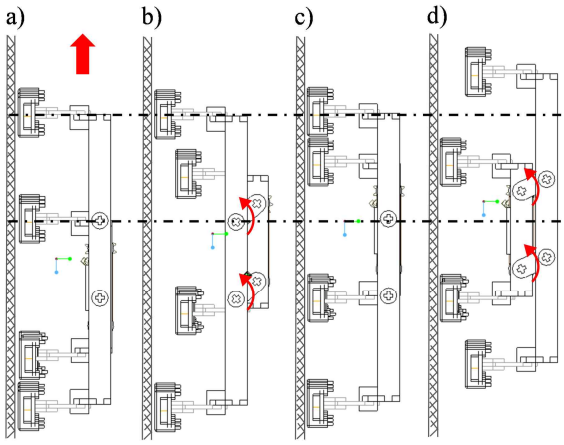


Fig. 2. Walking locomotion of wall climbing by parallel four-bar mechanism: a) initial position, b) inner frame moved, c) inner frame moved one step, and c) outer frame moved. Red arrows denote the rotational direction of the frames and moving direction of the robot.

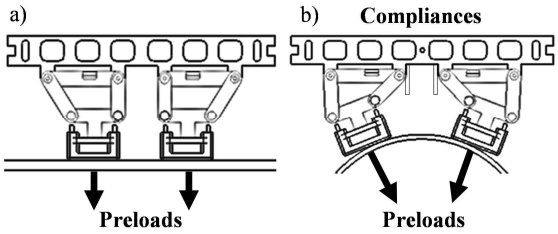


Fig. 3. Adaptation strategy on curved wall using a compliance structure: a) on a flat surface and b) on a curved surface. Preloads are very important for generating sufficient adhesion force for dry adhesives.

## III. Optimization of Dry Adhesive Footpads

### A. Problem definition

The dry adhesive footpads were optimized for adhesion ability on various curvatures. The footpads should adhere reliably to flat and curved walls for stable vertical climbing. The flat dry adhesive used is Vytaflex-10 elastomer (V-10, Smooth-on Inc.), which was successfully validated as an adhesive for WCRs [11, 12]. Since the V-10 elastomer is a pressure-sensitive adhesive, the generation of sufficient preloads is very important. In AnyClimb, the preloads are generated by the compliant adaptation mechanism presented in Section II. However, even with the mechanism, robust adhesion performance of the V-10 is also very important for stable vertical climbing.

The objective of the optimal design is to find the parameters that generate the same adhesion force as the preloading force. Since AnyClimb walks vertically based on repeated attachment and detachment, the optimal condition for stable climbing is when the preloading and adhering forces are the same. Three different radiuses of curvature are considered: $r = \infty$ (flat), 500, and 50 mm. The footpads should guarante robust adhesion force on these curvatures. The objective function for the experimental design is selected based on the signal-to-noise

This article has been accepted for publication in a future issue of this journal, but has not been fully edited. Content may change prior to final publication. Citation information: DOI 10.1109/TMECH.2016.2529664, IEEE/ASME Transactions on Mechatronics



(SN) ratio using Taguchi methodology [21] as follows:

$$SN = -10\log\left|\frac{E_{\infty}{}^2 + E_{500}{}^2 + E_{50}{}^2}{3}\right| [dB], \quad (1)$$

where $E_i$ denotes the difference between the adhesion and the preloading force for radius of curvature $i$ while a force of 2.695 N (0.275 $kg \cdot f$) is applied as the preload. From the definition of the SN ratio, the objective function can increase the average and deviation of the three forces at the same time [21].

Four design parameters were selected, as shown in Fig. 4: the shape, area, and thickness of the adhesive, and the thickness of the foam. The initial parameter candidates are summarized in Table 1. Figure 5 shows the experimental setup and an example of measured data. A load cell with a linear guide was used to measure the preloads and adhesion force, as shown in Fig. 5(b). The attaching and detaching speed was fixed at 50 mm/s.

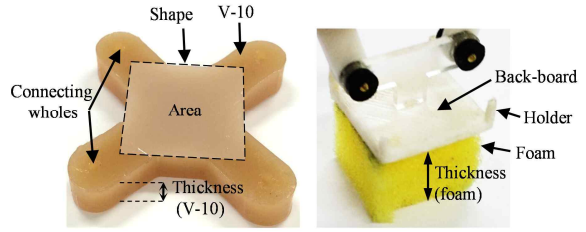


Fig. 4. Specification and design parameters of the footpad. Assembled footpad is indicated in Fig. 14. C.

Table 1
DESIGN PARAMETERS OF THE FOOTPADS

| Stage | First | | | Second | | |
|---|---|---|---|---|---|---|
| Parameters | Level | | | Level | | |
| | 1 | 2 | 3 | 1 | 2 | 3 |
| Shape | Square | Circle | Ellipse | - | - | - |
| Area ($cm^2$) | 1 | 2 | 3 | 3 | 4 | 5 |
| Thickness (V-10, mm) | 1 | 3 | 5 | 5 | 6 | 7 |
| Thickness (foam, mm) | 5 | 10 | 15 | - | - | - |

## B. Optimization results

For the four different design parameters, experiments were performed based on an orthogonal array of $L_9(3)$ [21] in two stages [22]. Figure 6 shows the sensitivity analysis results for the two-stage experimental design, where circle-pointed lines denote the first stage and square-pointed lines denote the second stage. Based on the results of the first stage, the area and the thickness of the V-10 were selected as the more sensitive parameters among the four candidates. The square shape shows the most robust performance among the shapes. The area and thickness of the V-10 show effects proportional to the adhesion performance. The kinematic parameters of the area and thickness are determined by the most sensitive parameters among the design parameters. The prototype was assembled based on the results of optimization, as shown in Section VI.

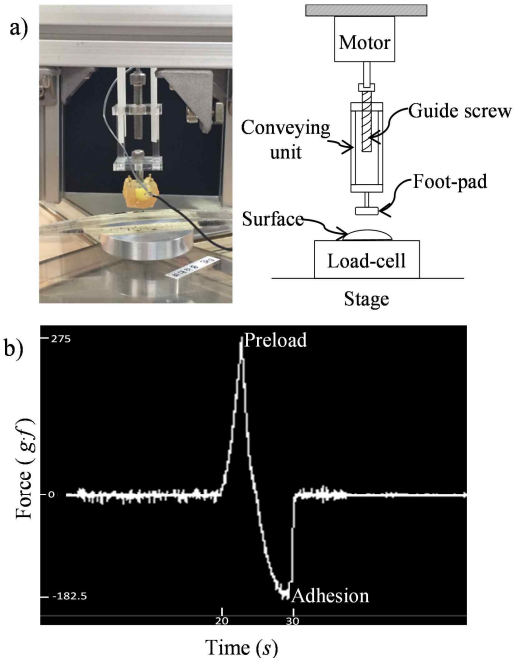


Fig. 5. Experimental setup: a) measurement setup by load-cell and b) experimental data of preloads and adhesion.

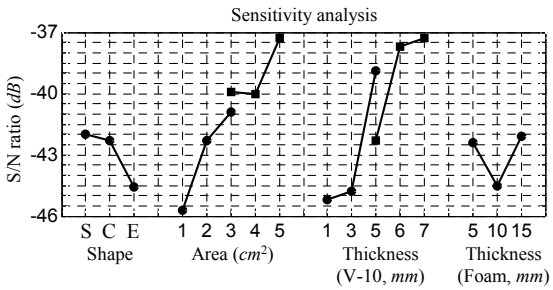


Fig. 6. Sensitivity analysis results on the design parameters of the footpads. In the parameters of the shape, S: square, C: circle, E: ellipse.

# IV. PARAMETER DESIGN

## A. Kinematic parameters

The kinematic lengths of the trapezoidal four-bar mechanism are very important for adapting to various curvatures. The parameters are determined based on the kinematic relations such as interference between each link. We also considered that the foot-pad could be horizontal at initial position. For designated parameters, the minimum radius of curvature which the robot could climb is determined as about 34mm like Fig. 7. However, in this research, we use the surfaces which radius of curvature is from 50mm to infinity to confirm the performance of the robot on the curved surface. Figure 7 shows the geometric configuration used to calculate the kinematic parameters of the adaptation mechanism.

The position kinematics of the four-bar linkages are defined by a loop-closure equation using complex vectors as follows:

$$l_1 e^{i\theta_1} + l_2 e^{i\theta_2} + l_3 e^{i\theta_3} + l_4 e^{i\theta_4} = 0, \quad (2)$$

This article has been accepted for publication in a future issue of this journal, but has not been fully edited. Content may change prior to final publication. Citation information: DOI 10.1109/TMECH.2016.2529664, IEEE/ASME Transactions on Mechatronics



where $l_i$ is the length of a link and $\theta_i$ is the angle of the link. In the design process, $l_1$ and $l_2$ are fixed and $\theta_1$ is zero. $l_2$ is designed to achieve a small height to minimize the pitch-back moment. $\theta_3$ is determined from the objective radius of curvature, $r$ = 50 mm. The lengths of $l_3$ and $l_4$ are determined based on the given information. From Eq. (2), the angles between each link, $\theta_2$ and $\theta_3$, can be determined simply from the given radius of curvature of the surface. $\theta_2$ is an important factor for determining the compliance force, and the compliance parameter should be determined.

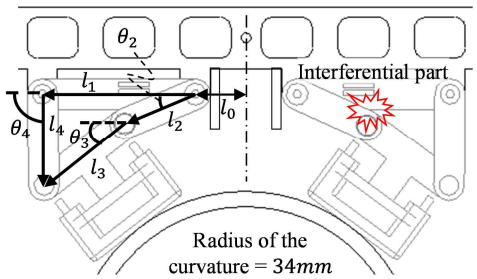


Fig. 7. Geometric configuration to determine the kinematic parameters of the adaptation mechanism ($l_0$ = 20.5 mm, $l_1$ = 30 mm, $l_2$ = 15 mm, $l_3$ = 20 mm, and $l_4$ = 18.03 mm). Minimum radius of curvature which the robot could climb is 34mm because $l_1$ and $l_3$ which are located in the same plane interfere each other.

## B. Compliance parameters

The compliance of the trapezoidal four-bar linkage is important for recovering the position after detaching. If the initial position of the linkage cannot be completely recovered, repeated adhesion and detachment are not possible. A torsional spring is implemented between links $l_1$ and $l_2$ to generate the compliance force. Reasonable selection of the spring constant is necessary for stable vertical climbing.

Figure 8 shows the forces in the attachment and detachment procedures. The torque of the motor is applied to detach the footpads against the adhesion force when the linkage moves upward. At the same time, the torque of the spring generates preloads on the footpads, as in Fig. 8(a). When the linkage moves downward as in Fig. 8(b), the adhesion force $F_a(i+1)$ is determined by the adhesion force $F_a(i)$ from the footpads of the other frame, as well as the torque of the spring-generated preloads on the footpads and the preload. We assume that the adhesion force of detachment is transferred to the preload of attachment. This procedure is sequentially calculated for the footpads of the inner and outer frames.

To determine the adhesion force, the characteristics of the V-10 adhesive should be defined. The V-10 adhesion characteristics on a smooth surface are defined as a function of the preload as follows [12]:

$$p_a = A\left(p_p\right)^B \tag{3}$$

where $p_a$ is the adhesion pressure and $p_p$ is the preload pressure. The constants $A$ and $B$ are determined experimentally as 13.67 and 0.13, respectively, using a V-10 thickness of 7 $mm$.

Figure 9(a) shows the detailed calculation procedure of the adhesion force, which is done iteratively based on the force equilibrium equation with the kinematics. Figure 9(b) shows the results on the vertical climbing on a flat surface. Even though the adhesions are reduced due to weight of the robot as pitch-back moment, the force of the tail compensates the reduced adhesions, and the adhesion of each footpad is consistently maintained at certain values respectively when the stiffness of the spring is $5\times10^{-4}$ $N{\cdot}m/rad$. The footpads successfully repeat attachment and detachment sequentially in the simulation.

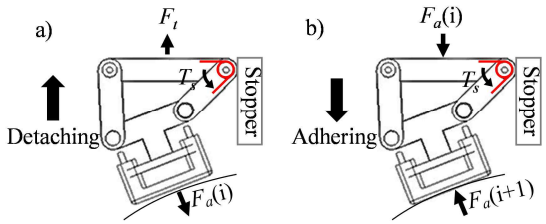


Fig. 8. Posture to design the compliance parameters: a) during detachment and b) during attachment. $F_t$ is the torque of the motor to detach the adhesion, $T_s$ is the torque of the torsional spring, and $F_a$ is the adhesion. Red lines denote the torsional spring attached to $L_2$ and $L_1$.

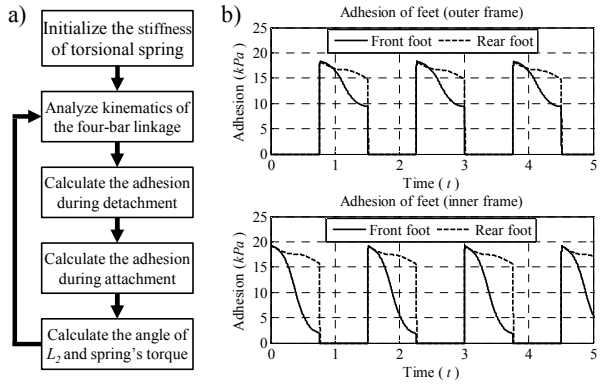


Fig. 9. Calculation procedure and the results: a) iterative calculation procedure of the adhesion force and torque on the spring and b) calculated adhesion forces of the footpads. Footpads of inner and outer frames repeat the walking in vertical direction (flat surface, force of the tail = 1$kPa$).

When the robot climbs on a curved surface, the footpads are peeled off during detachment because of the trapezoidal linkage and torsional spring. Some of the overall forces to detach the foot pad are consumed as peeling forces, and the transported forces as a preload of other feet is reduced. The peeling force is increased as the peeling angle between the tangential direction of the surface and surface of the foot is increased because the peeling force is a function of the peeling angle. For this reason, the saturated adhesion is reduced as the radius of the curvature is reduced. The peeling force $F_p$ can be calculated as follows [24]:

$$\left(\frac{F_p}{w}\right)^2 \frac{1}{2tE} + \left(\frac{F_p}{w}\right)\left(1-\cos\theta_p\right) - R = 0 \tag{4}$$

where $w$ is the width of the footpad (22.4 mm), $t$ is its thickness (7 mm), $E$ is the Young's modulus of V-10, and $R$ is the adhesive energy of the elastomer. $E$ and $R$ were empirically

This article has been accepted for publication in a future issue of this journal, but has not been fully edited. Content may change prior to final publication. Citation information: DOI 10.1109/TMECH.2016.2529664, IEEE/ASME Transactions on Mechatronics



measured as 110 kPa and 70 N/m, respectively, on an acrylic surface with a pulling speed of 2 mm/s [25].

The moving distance during one period of the foot is $\pi\times$30mm and taken time during this period is nearly 1.7 *s*. Therefore, the peeling speed of the foot is nearly 50 mm/s. The peeling angle $\theta_p$ is defined by considering the torque of $l_3$ in Fig. 6 generated by the adhesion, torsional spring, and torque of the motor. Fig. 10 shows the variation of saturated adhesion according to the radius of the curvature. The adhesion of the each foot are reduced as the radius of the curvature is increased because the energy loss increases with the higher curvature like the equation (4). More specific explanation about difference of adhesion of the feet is explained in Section VI. B (Fig. 18).

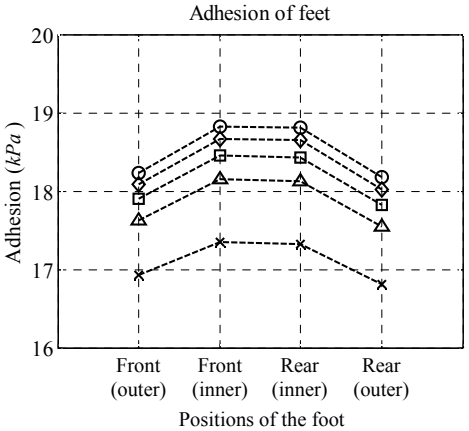


Fig. 10. Relation between the radius of the curvatures and the adhesion forces when the stiffness of the spring is $5\times10^{-4}$ $N\cdot m/rad$. Force of the tail is 1*kPa*. Mark styles denote the radius of the curvature: circle: infinity, diamond: 150mm, square: 100mm, triangle: 75mm, and x-mark: 50mm.

The adhesion according to the stiffness of the spring is indicated in Fig. 11. The adhesion force is decreased as the stiffness of the spring is increased because of the contact angle between the foot and tangential direction of the surface. The high stiffness makes the mechanism less flexible. For this reason, the preload forces are consumed by the tangential contact between the foot and surface. The compliance is essential for moving the linkage to the initial position and its value should be larger than zero. In the prototype, we selected a spring with a small stiffness of $5\times10^{-4}$ $N\cdot m/rad$.

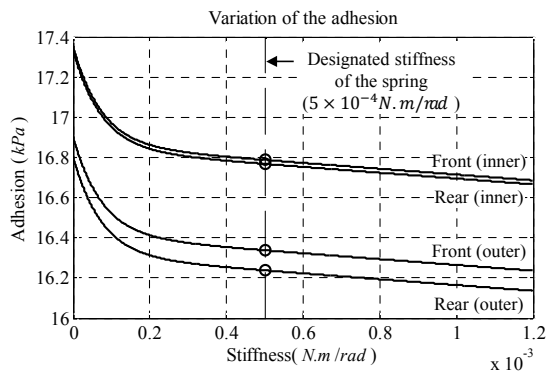


Fig. 11. Relation between the stiffness of the torsional spring and the adhesion forces when the robot climbs on a curved surface (r =50 mm). Circles denotes the designed value.

## V. FAILURE ANALYSIS

The failure conditions should be checked for stable climbing. Vertical climbing has two failure modes: falling and slipping. Falling happens when the pitch-back moment generated is high enough to detach the footpads, and slipping happens when the friction force is not sufficient to maintain the weight in the vertical direction. These falling modes can be prevented by the forces of the tail ($F_t$) like in Fig. 12. And force of the tail used for simulation and experiment in this research is 1kPa as a similar unit of adhesion.

Fig. 12 shows the free body diagram used to study the failure conditions. The two worst postures were selected to find the extreme conditions of failure. The failure conditions from the two postures are defined as follows:

Falling:

$$F_{of}l_o + F_t l_t < m_i g(h_f + h_l) + m_o g h_f , \tag{5}$$

$$F_{if}l_i + F_t(l_t + \frac{l_o - l_i}{2}) < m_i g h_f + m_o g(h_f + h_l) , \tag{6}$$

Slipping:

$$f_{of} + f_{or} < m_i g + m_o g , \tag{7}$$

$$f_{if} + f_{ir} < m_i g + m_o g . \tag{8}$$

The falling conditions can be examined simply by using an adhesion force calculated in IV. B (Fig. 10). Capacity for payload is calculated by the falling condition, and it is suggested in Fig. 20. To investigate the slipping conditions, the friction force should be calculated first. The friction of the elastomer is defined as follows:

$$f = \mu N_i + \tau A , \tag{9}$$

where $\mu$ is the friction coefficient, $N_i$ is the surface normal force, $\tau$ is the shear strength, and $A$ is the contact area. $\mu$ and $\tau$ are given as 2 and 0.125 kPa from previous research [9]. Here, the surface normal force can be calculated by the moment equilibrium equations as follows:

$$N_{of} = \frac{-m_i g h_f - m_o g(h_f + h_l) + F_t l_t}{l_o} , \tag{10}$$

$$N_{or} = \frac{m_i g h_f + m_o p(h_f + h_l) - F_t(l_o + l_t)}{l_o} , \text{ and} \tag{11}$$

$$N_{if} = \frac{-m_o g h_f - m_i g(h_f + h_l) + F_t(l_t + (l_o - l_i)/2)}{l_o} , \tag{12}$$

$$N_{ir} = \frac{m_i g h_f + m_o p(h_f + h_l) - F_t(l_t + (l_o + l_i)/2)}{l_o} . \tag{13}$$

We can check the slipping condition based on the normal force calculation in the force equilibrium equation. The equations indicate that the masses of the inner and outer frames should be constrained. Note that $m_i$ is larger than $m_o$ in the AnyClimb design since the motor is equipped on the inner frame.

This article has been accepted for publication in a future issue of this journal, but has not been fully edited. Content may change prior to final publication. Citation information: DOI 10.1109/TMECH.2016.2529664, IEEE/ASME Transactions on Mechatronics



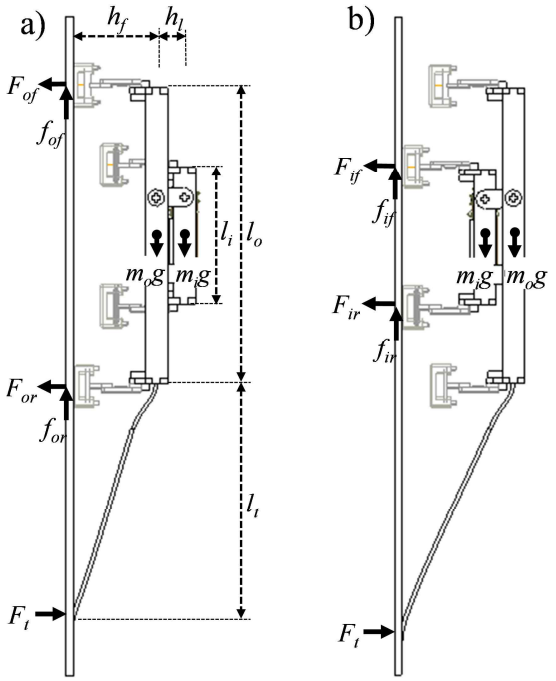


Fig. 12. Free body diagram for failure analysis: a) when inner frame is moved and b) when outer frame is moved. $F_{of}$, $F_{or}$, $F_{if}$, and $F_{ir}$ are the adhesion forces on the outer and inner frames. $f_{of}$, $f_{or}$, $f_{if}$, and $f_{ir}$ are the friction forces on the footpads. $l_i$, $l_o$, and $l_t$ are the lengths of the inner and outer frames and tail. $h_f$ and $h_i$ are the heights of the frame and four-bar linkages. $m_i$ and $m_o$ are the masses of each frame.

## VI. Experimental Results

### A. Prototype

A prototype was assembled as shown in Fig. 13. The main frame was made with acrylic plates of 3-mm thickness. A single DC motor (298:1 Mini Metal Gear Motor, Solarbotics) is equipped in the middle of the inner frame. The size of the prototype is 114($w$) × 200 ($l$) × 60 ($h$) mm$^3$ without the tail, and its weight is 142 g. A torsional spring with a stiffness of $5\times10^{-4}$ $N{\cdot}m/rad$ is used to achieve compliance in the trapezoidal four-bar mechanism. Power is provided by an external DC supply. The design parameters are summarized in Table 2. Since the motor is equipped in the inner frame, $m_i$ is larger than $m_o$. The values are used to analyze the failure conditions in Section V, and all conditions are successfully satisfied.

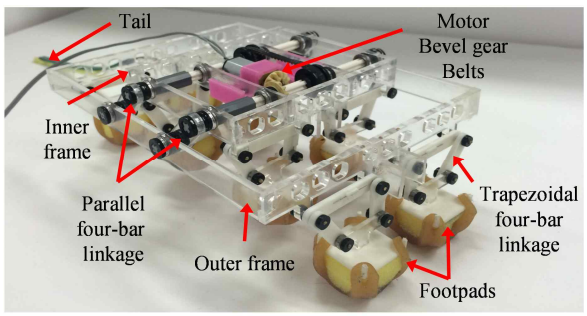


Fig. 13. Photograph of the robot prototype.

Table 2
Parameters of the Prototype

| Parameters | Values | Parameters | Values |
|---|---|---|---|
| $m_o$ | 59 $g$ | $m_i$ | 83 $g$ |
| $l_o$ | 152 $mm$ | $l_i$ | 72 $mm$ |
| $h_f$ | 50 $mm$ | $h_l$ | 15 $mm$ |
| $l_t$ | 144 $mm$ | | |

The eight V-10 footpads were manufactured by a molding and laser-cutting process. Figure 14(a) shows the detailed procedure of the fabrication process. Firstly, we mixed the two components of V-10 and stirred them (Figs. 14(a-1) and (a-2)). After de-gassing the mixed V-10, it was cured for a day in ambient conditions (Fig. 14(a-3)). The footpad shape was made using a laser cutting machine (Figs. 14(a-4) and (b)). The V-10 footpads were used after cleaning with ethyl alcohol.

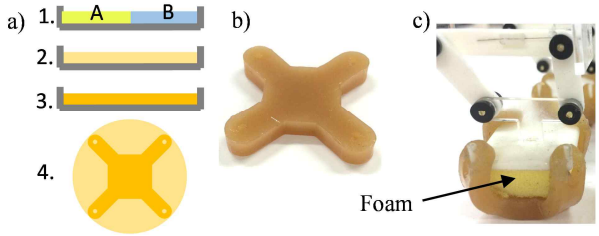


Fig. 14. Fabrication process of V-10 footpads. a) Fabrication process and b) manufactured V-10 footpad. c) Assembled footpad.

### B. Flat and curved wall climbing

Figs. 15 and 16 show the experimental results of vertical climbing on a flat surface and curved surface, respectively. Acrylic surfaces are selected to make very smooth surfaces. The compliance mechanism adapts well to the flat and curved surfaces, as shown in Figs. 15 and 16 (e)–(h). The climbing experiments were performed on more surfaces with different radiuses of curvature of r = 50, 75, 100, and 150 $mm$, and we obtained successful results on the surfaces. Please see the videos in the multimedia extension.

For each climb, speeds of 1.25 cm/s on the flat surface and 0.83 cm/s on the curved surface were achieved by the proposed walking mechanism. The reason for the different climbing speeds is that more time is taken for detachment on the curved surface than on the flat surface. The detachment force generated by the motor is divided into the tangential and normal directions to the surface. The detaching occurred from the force in the normal direction and it is reduced as the radius of curvature is decreased. For this reason, the detaching takes more time as the curvatures of the surface decrease, and increasing the detaching time makes the climbing speed low. The results of the experiment are indicated in Fig. 17.

Maintaining position is also very important for inspection operations. The capacity of the robot to maintain its position is limited to several minutes after stopping the motor. The loitering time can be improved by an adhesion recovery algorithm [16].

This article has been accepted for publication in a future issue of this journal, but has not been fully edited. Content may change prior to final publication. Citation information: DOI 10.1109/TMECH.2016.2529664, IEEE/ASME Transactions on Mechatronics



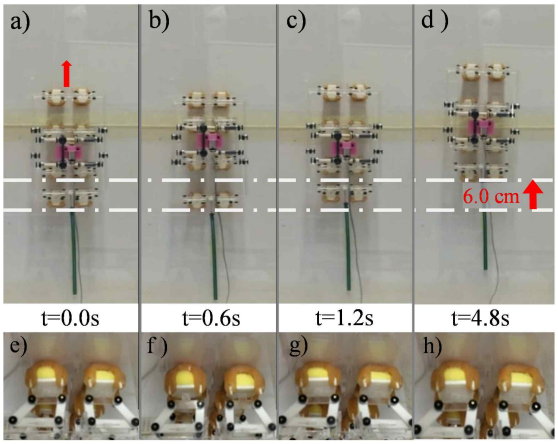


Fig. 15. Photos of vertical climbing on a flat surface. (a) – (d) The inner and outer frames moved one step in the vertical direction. (e) – (h) Top view of each posture. (Please see the multimedia extension.)

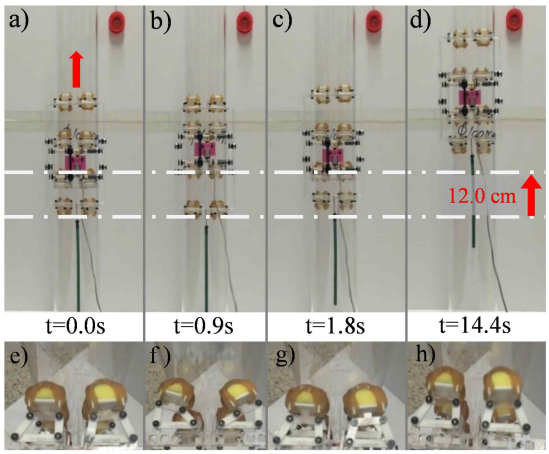


Fig. 16. Photos of vertical climbing on a curved surface with r = 50 mm. (a) – (d) The inner and outer frame moved one step in the vertical direction. (e) – (f) Top view of each posture. The compliance mechanism successfully adapts to the curved surface. (Please see the multimedia extension.)

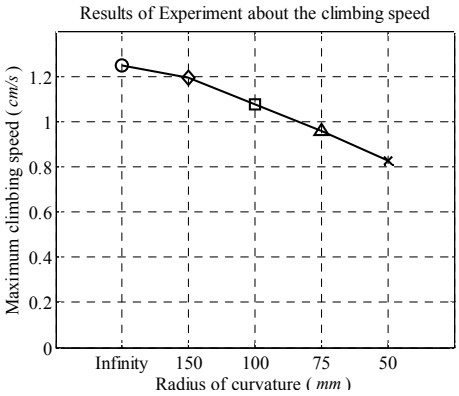


Fig. 17. Results of the experiment with respect to the climbing speed on five curvatures. Mark styles denote the radius of the curvature: circle: infinity, diamond: 150mm, square: 100mm, triangle: 75mm, and x-mark: 50mm.

The adhesion was also measured during climbing the surfaces of flat, 150mm and 50mm radius. Experimental equipment and measured data are suggested in Fig. 18. Classified results of simulation with respect to the various curvatures are indicated in Fig. 10 and 19. The experimental equipment is simply designed. Each surface has separated parts like closed-red line in the Fig. 18(a). The separated area is connected with load cell (651AM, KTOYO) attached with overall frame.

In the results, the forces of the tail in three experiment are the same as $1kPa$. The adhesion of the feet in the outer frame is smaller than inner frame's feet. This is because the front foot in the outer fame receives more effect as the pitch-back moment than inner frame's feet due to the higher weight of inner frame. The inner frame contains weight of a motor and other parts which transmit power. The rear foot in the outer frame receive the effect caused by force in the vertical direction of the tail. This force is not the force of pitch-back moment, it is just transmitted reaction force between the tail and surface when the tail touch the surface. However, effect of this reaction force is relatively small in the rear foot in the inner frame. For these reasons, the measured adhesion in the inner frame are larger than outer frame's feet.

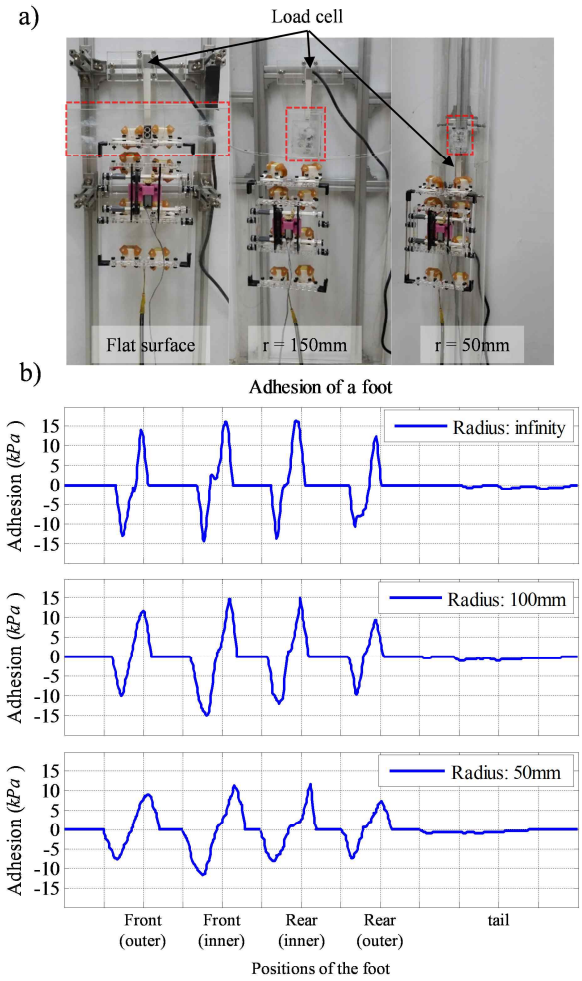


Fig. 18. Experiment to measure the adhesion for three kinds of curvature. a) Experimental equipment. The closed-red area indicates measuring area connected with load cell. b) Measured data when the robot climbs vertical surface (force of the tail = $1kPa$).

This article has been accepted for publication in a future issue of this journal, but has not been fully edited. Content may change prior to final publication. Citation information: DOI 10.1109/TMECH.2016.2529664, IEEE/ASME Transactions on Mechatronics



As another characteristic in this result, time during the attachment and detachment process is increased as the radius of the curvature decreases. This is because more time is consumed due to the peeling forces and rotation of four-bar mechanism. With the consumed time, the adhesion is decreased. Loss of adhesion due to the peeling force make reduction of adhesion. These results are indicated in Fig. 19.

In the Fig. 19, the measured data is smaller than simulation. There are some reasons to explain this difference such as condition of foot pad's surface and attached area of the foot. Among these reasons, we believe that the alignment issue is the main problem for the error.

We would like to discuss the alignment issue to a vertical direction on a curved surface. From the symmetric compliant design of the AnyClimb, we expect the self-alignment ability of the robot when there is little error in yaw direction. To prove the hypothesis, many tests were performed by setting-up the robot to have yaw directional error to the vertical direction, and investigated the self-aligning characteristic. However, from the empirical result, the robot was proven not to have self-alignment ability. This is because the robot's legs are folded independently, and there is no symmetric force to make the robot to be aligned to the vertical direction. Because of the minimal and compliant design of AnyClimb, there is no possibility to make the robot have self-alignment ability in the design, and this is a limitation of the AnyClimb design. Note all the experiments have been performed after precise vertical alignment.

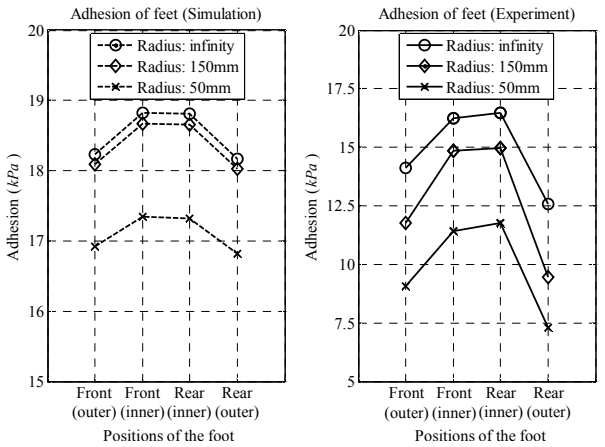


Fig. 19. Measured adhesion of the feet with respect to the radius of the surface.

### C. Payload capacity

We also conducted an experiment to test the capacity for carrying a payload during vertical climbing on a flat surface and curved surface. The payload was attached at the point connecting the tail to the outer frame, and the interval of payload is 5 g. The position of the torque generated by the payload has nothing to do with the falling and slipping conditions because the torque is determined by the payload and distance between the wall and the position of the payload. So, the torque is the same whether the payload is attached at the front or back parts of the robot. The experiment was repeated until the robot fell and slipped on the surface with increasing payloads. These two conditions with respect to the falling and slipping were defined in Section V, and we tested them experimentally, and they are compared with results of simulation.

As shown in Fig. 20, in the two results, the capacity for the payload is decreased as the radius of the surface is decreased. As mentioned in Section VI. B, the adhesion is reduced due to the peeling forces. For this reason, the adhesion in measured data and results of simulation are decreased with the radius of the curvature as mentioned earlier. In addition, the increasing the payload causes additional reduction of adhesion, and eventually, the foot lose their adhesion. The process of losing the adhesion occurs in regular sequence from front foot in the outer frame to rear foot in the inner frame except the rear foot in the outer frame because the outer frame's rear foot is considered as center of rotation when the robot climbs the vertical surface. So, we considered this process in the simulation.

The measured payloads were smaller than the payloads calculated from the simulation. The reasons for this difference can be also explained as condition and attached area of the foot. We think that alignment issue is the most crucial factor for this difference as mentioned in Section VI. B.

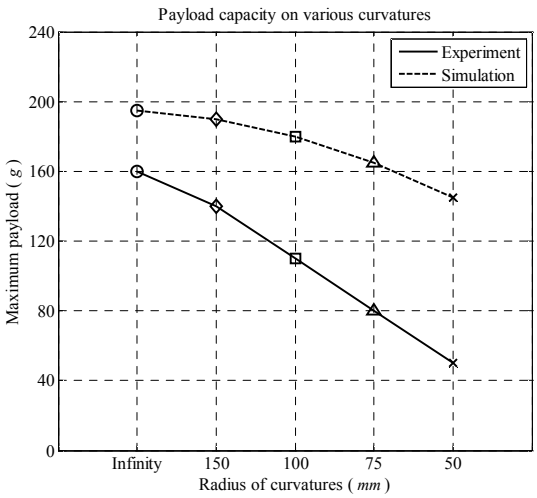


Fig. 20. Results of the payload capacity on five curvatures. Mark styles denote the radius of the curvature: circle: infinity, diamond: 150mm, square: 100mm, triangle: 75mm, and x-mark: 50mm.

## VII. Conclusions

This paper proposed a new climbing robot platform named AnyClimb for surfaces with various curvatures, such as walls and poles. AnyClimb consists of a walking mechanism for vertical movement and a compliant mechanism for horizontal adaptation to a curved wall. Flat dry adhesive footpads were implemented for attachment to the wall, and the footpad shape and geometry were optimized by experiments. To adapt to the curved wall successfully, kinematic and compliance parameters

were determined analytically. Failure analysis was conducted on falling and slipping modes to verify the stability of vertical climbing. Experiments were performed on walls with different curvature, including a flat wall and a pole with 50-mm radius, and the climbing ability was done successfully. In addition, an experiment was performed for the payload capacity, which decreased as the wall curvature decreased. The AnyClimb platform is initial research to develop a robust climbing robotic platform for unstructured surfaces for various applications, such as inspection and exploration. As a future work, we have a plan to control the yawing direction when the robot climbs vertical surfaces. By the controlling the yawing direction, the robot is going to able to steering locomotion and self-stabilization.

## REFERENCES


[1] Serbot AG – Solar panel cleaning and façade cleaning, http://www.serbot.ch/ (retrieved at 11/18/2014).

[2] Urakami Painting robot (water tank), http://www.urakami.co.jp/en/05/11.html (retrieved at 11/18/2014).

[3] G. Lee, H. Kim, K. Seo, J. Kim, M. Sitti, T. Seo, Series of Multi-linked Caterpillar Track-Type Climbing Robots, *Journal of Field Robotics*, Online Published, DOI: 10.1002/rob.21550 (2015).

[4] Y. Mengüç, M. Röhrig, U. Abusomwan, H. Hölscher, M. Sitti, Staying sticky: contact self-cleaning of gecko-inspired adhesives, *Journal of Royal Society Interface*, 11(94) (2014)

[5] J. Song, Y. Megnuc, M. Sitti, Enhanced fabrication and characterization of gecko-inspired mushroom-tipped microfiber adhesives, *Journal of Adhesion Science and Technology*, 27(17) (2013) 1921-1932.

[6] J.-S. Kwak, T.-W. Kim, A review of adhesion and friction models for gecko feet, *International Journal of Precision Engineering and Manufacturing*, 11(1) (2010) 171-186.

[7] L. R. Palmer, E. Diller, R. D. Quinn, Toward gravity-independent climbing using a biologically inspired distributed inward gripping strategy, *IEEE/ASME Trans. on Mechatronics*, 20(2) (2014) 631-640.

[8] A. Parness, C. McKenzie, DROP: the durable reconnaissance and observation platform, *Industrial Robot: An International Journal*, 40(3) (2013) 218-223.

[9] F. Xu, X. Wang, G. Jiang, Design and Analysis of a Wall-Climbing Robot Based on a Mechanism Utilizing Hook-Like Claws, *International Journal of Advanced Robotic Systems*, 9 (2012) 1-12.

[10] A. Sintov, T. Avramovich, A. shapiro, Design and motion planning of an autonomous climbing robot with claws. *Robotics and Autonomous Systems*, 59(11) (2011) 1008-1019.

[11] T. Seo, M. Sitti, Tank-Like Module-Based Climbing Robot Using Passive Compliant Joints, *IEEE/ASME Trans. on Mechatronics*, 18(1) (2013) 397-408.

[12] O. Unver, M. Sitti, Flat dry elastomer adhesives as attachment materials for climbing robots, *IEEE Transaction on Robotics*, 26(1) (2010) 131–141.

[13] B. He, Z. Wang, M. Li, K. Wang, R. Shen, S. Hu, Wet adhesion inspired bionic climbing robot, *IEEE/ASME Trans. on Mechatronics*, 19(1) (2014) 312-320.

[14] B. Chu, K. Jung, C.-S. Han, D. Hong, A survey of climbing robots: Locomotion and adhesion, *International Journal of Precision Engineering and Manufacturing,* 11(4) (2010) 633-647.

[15] M. J. Spenko, G. C. Haynes, J. A. Saunders, M. R. Cutkosky, A. A. Rizzi, R. J. Full, D. E. Koditcheck, Biologically inspired climbing with a hexapedal robot, *Journal of Field Robotics*, 25(4-5) (2008) 223-242.

[16] M. Murphy, M. Sitti, Waalbot: An Agile Small-Scale Wall Climbing Robot Utilizing Pressure Sensitive Adhesives, *IEEE/ASME Trans. on Mechatronics*, 12(3) (2007) 330-338.

[17] S. H. Lee, Design of the out-pipe type pipe climbing robot, *International Journal of Precision Engineering and Manufacturing*, 14(9) (2013)1559-1563.

[18] K. H. Cho, H. M. Kim, Y. H. Jin, F. Liu, H. Moon, J. C. Koo, H. R. Choi, Inspection robot for hanger cable of suspension bridge: mechanism design and analysis, *IEEE/ASME Trans. on Mechatronics*, 18(6) (2013) 1665-1674.

[19] G. C. Haynes, A. Khripin, G. Lynch, J. Amory, A. Saunders, A. A. Rizzi, D. E. Koditscheck, Rapid pole climbing with a quadrupedal robot, *in Proc. of IEEE International Conference on Robotics and Automation*, Kobe, Japan, 2009, pp. 2767-2772.

[20] Y. Guan, L. Jiang, H. Zhu, X. Zhou, C. Cai, W. Wu, Z. Li, H. Zhang, X. Zhang, Climbot: A modular bio-inspired biped climbing robot, *In Proc. of IEEE/RSJ International Conference on Intelligent Robots and Systems*, San Francisco, USA, 2011, 1473-1478.

[21] Taguchi, G., *Taguchi on Robust Technology Development: Bringing Quality Engineering Upstream*, ASME Press, pp. 273-291, 1993.

[22] Y. Liu, M. Shin, T. Seo, "Optimization design of dry adhesion for wall-climbing robot on various curvatures based on experiment," *Journal of the Korean Society of Manufacturing Technology Engineers*, 23(4) (2014) 398-402.

[23] V-10 elastomer, Smooth-on Inc., Retrieved Jan. 8, 2015, from http://www.smooth-on.com.

[24] K. Jendal, "Thin-film peeling-the elstic term," *J. Phys. D, Appl. Phys*., vol. 8, pp. 1949-1952, 1975.

[25] O. Unver and M. Sitti, "A miniature ceiling walking robot with flat tacky elastomeric footpads," *in Proc. IEEE Int. Conf. Robot. Autom*., Kobe, Japan, 2009, pp. 2276-2281.


**Yanheng Liu** received her B.S. and M.S. degrees from the School of Mechanical Engineering, Yeungnam University, Korea, in 2013 and 2015, respectively, where he is currently working toward a Ph.D. Her research interests include climbing robot design, dry adhesive fabrication, and Taguchi methodology.

**HyunGyu Kim** received his B.S. and M.S. degrees from the School of Mechanical Engineering, Yeungnam University, Korea, in 2014 and 2016, respectively. His research interests include the design and analysis of bio-inspired robots and control.

**TaeWon Seo (M'10)** is an Assistant Professor in the School of Mechanical Engineering, Yeungnam University, Gyeongsan, Korea. He received his B.S. and Ph.D. degrees in the School of Mechanical and Aerospace Engineering, Seoul National University, Korea, in 2003 and 2008, respectively. He was a Post-Doctoral Researcher at the Nanorobotics Laboratory, Carnegie Mellon University, PA, USA in 2009, and Visiting Researcher at the Biomimetic Millisystems Laboratory, UC Berkeley, CA, USA in 2015. His research interests include creative robotic platform design, control, optimization, and motion planning. Dr. Seo received the Best Mechatronics Paper Award of the IEEE/ASME Transaction on Mechatronics in 2014.